THE JOURNAL OF PHYSICAL CHEMISTRY Letters

pubs.acs.org/JPCL Letter

Liquid–Liquid Phase Separation Produces Fast H-Bond Dynamics in DMSO–Water Mixtures

Kwang-Im Oh,[†] Xiao You,[†] Jennifer C. Flanagan, and Carlos R. Baiz*

Cite This: *J. Phys. Chem. Lett.* 2020, 11, 1903–1908 Read Online

ABSTRACT: Liquid–liquid phase separation is common in complex mixtures, but the behavior of nanoconfined liquids is poorly understood from a physical perspective. Dimethyl sulfoxide (DMSO) is an amphiphilic molecule with unique concentration-dependent bulk properties in mixtures with water. Here, we use ultrafast two-dimensional infrared (2D IR) spectroscopy to measure the H-bond dynamics of two probe molecules with different polarities: formamide (FA) and dimethylformamide (DMF). Picosecond H-bond dynamics are fastest in the intermediate concentration regime (20–50 mol % DMSO), because such confined water exhibits bulk-like dynamics. Each vibrational probe experiences a unique microscopic environment as a result of nanoscale phase separation. Molecular dynamics simulations show that the dynamics span multiple time scales, from femtoseconds to nanoseconds. Our studies suggest a previously unknown liquid environment, which we label "local bulk", in which despite the local heterogeneity, the ultrafast H-bond dynamics are similar to bulk water.

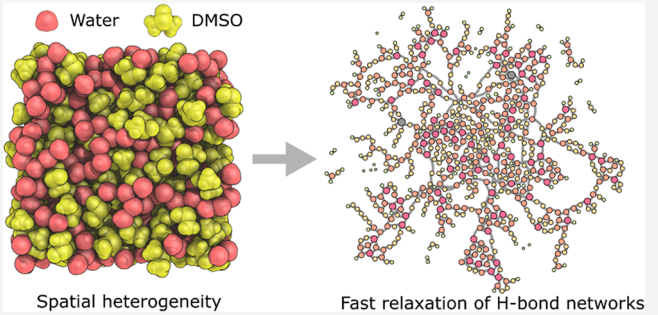

Microscopic heterogeneity is common in aqueous mixtures of alcohols,[1−4] amides,[5] or dimethyl sulfoxide (DMSO).[6,7] Phase separation is postulated to play a role in partitioning biomolecules;[8−11] indeed, life is theorized to have originated from a coacervate of aqueous organic molecules.[1,11−14] Unlike simple solutions where a solute experiences uniform solvation, heterogeneity produces a gradient of environments causing solutes to partition into different microenvironments. Heterogeneous liquids have received significant attention because clustering and phase separation remain challenging to access experimentally and difficult to model.[15−21]

Among binary mixtures, DMSO–water solutions have received widespread attention because of their unusual bulk properties and common use as cryoprotectants.[22−24] Molecular packing, H-bond donor/acceptor imbalance, and DMSO's amphiphilic character produce highly concentration-dependent bulk properties such as viscosity,[25,26] density,[26] entropy of mixing,[27,28] diffusion rates,[29] and freezing points.[30] The origin of these properties has been investigated using neutron diffraction,[31,32] dielectric relaxation spectroscopy,[33,34] vibrational spectroscopy,[35−37] fluorescence,[38] NMR spectroscopy,[29] and molecular dynamics (MD) simulations.[39,40] Recently, we have quantified the equilibrium DMSO H-bond populations using a combination of IR spectroscopy and MD simulations, but obtaining a complete picture of the mixtures requires characterizing not only environments but also the liquid reorganization time scales.[41]

The overall dynamical heterogeneity of these mixtures remains unresolved because the measured dynamics depend on the probe.[7,29,39,42−45] For example, using two-dimensional infrared (2D IR) spectroscopy, Fayer and co-workers reported the changes in O–D spectral diffusion and orientational relaxation rates across the DMSO–water concentration range.[7] Roy and Bagchi found slower solvation dynamics at 10–20 mol % and 35–50 mol % DMSO.[39] Kashid et al. used a carbonyl probe showing a critical point at around 15 mol % DMSO, and more recently, slow dynamics around 35 mol % DMSO were measured using thiocyanate probes.[42] While initially these results might appear incongruous, each probe samples a different environment. Here, we demonstrate this phenomenon using ultrafast 2D IR spectroscopy on two different carbonyl probes with varying hydrophobicity. Each probe reveals different H-bond lifetimes and global heterogeneity, which shows that the DMSO–water mixtures produce a range of environments and each probe samples a unique environment. Ultrafast 2D IR spectroscopy is an ideal technique to measure H-bond dynamics.[5,46−48] Specifically, in this Letter we monitor the dynamics of two amides with similar chemical composition but varying hydrophobicity, formamide (FA) and

Received: February 4, 2020
Accepted: February 18, 2020
Published: February 18, 2020

https://dx.doi.org/10.1021/acs.jpclett.0c00378
J. Phys. Chem. Lett. 2020, 11, 1903–1908

dimethylformamide (DMF), to investigate H-bond networks and microscopic phase separation (Figure 1).

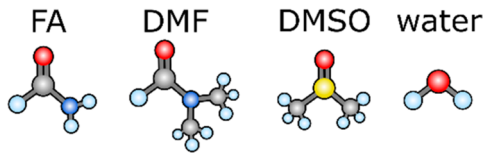

Figure 1. Molecular structures of formamide (FA), dimethylformamide (DMF), dimethyl sulfoxide (DMSO), and water.

Bulk Environments Measured by FTIR Spectroscopy. Figure 2 shows IR absorption spectra of dilute FA and DMF. Both species

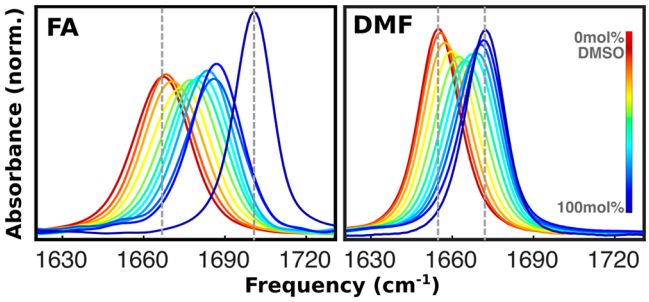

Figure 2. Carbonyl stretch IR absorption spectra of FA and DMF in DMSO/D_2O concentrations, from 0 mol % DMSO, or pure D_2O, to 100 mol % DMSO as indicated in the color bar. The vertical lines indicate the peak centers (see section S2).

exhibit a monotonic blue shift with increasing DMSO concentration. More specifically, FA blue shifts by 43 cm^{-1} and DMF by 15 cm^{-1} (Figure S2). Water-rich mixtures produce more red-shifted peaks as the number of H-bond donors is larger compared to DMSO-rich mixtures. In addition, the bulk polarity of the DMSO-rich mixtures is lower compared to that of water. Trends in peak width are more nuanced but generally increase at intermediate concentrations (20−60 mol % DMSO), suggesting an increase in the inhomogeneity of the solution.

Solvation Dynamics Measured by 2D IR Spectroscopy. Figure 3 shows representative carbonyl 2D IR spectra of FA in D_2O at different waiting times (section S3 and Figures S3 and S4). Short waiting times produce diagonally elongated peaks, which become rounder as the excitation-to-detection correlation is lost with increasing delay (Figure 3A−C). Nodal line slope (NLS) decays (Figure 3D,E) represent the frequency−frequency time correlation function $C(t)$, which is analyzed, together with the absorption lineshapes (Figures 2 and S2), using the standard Bloch model at each composition of the mixture:

$$C(t) = \langle \delta\omega(t)\delta\omega(0)\rangle = \frac{\delta(t)}{T_2} + \Delta^2 \exp\left(\frac{-t}{\tau}\right) + \Delta_0^2 \quad (1)$$

where Δ^2, τ, and Δ_0^2 correspond to the amplitude of frequency fluctuations, relaxation time constant, and the static inhomogeneity components, respectively (Figure 4). The constant T_2 gives rise to the homogeneous width. The relaxation time constant can be interpreted as the picosecond fluctuations of the local environment surrounding the C=O. In water-rich environments, these fluctuations are dominated by H-bond interactions, whereas in the DMSO-rich environments these local electric-field fluctuations result from the rearrangements of molecules within the first solvation shell.[49] The "static" inhomogeneity component, Δ_0^2, represents the line width contribution from environments that persist for longer than the 2D IR time scale (~3 ps). The inhomogeneous component (Figure 4B) reaches a maximum at ~50−60 mol % DMSO in both FA and DMF, although the inhomogeneity is larger overall for FA. This characteristic bell-shaped curve has been observed in numerous measurements, and its dependence on concentration is correlated with bulk solution properties such as density and viscosity.[7,29,44] Overall, the static inhomogeneity is small for pure water compared to the mixtures. In the 30−50 mol % range, both probes show increased inhomogeneity, as a result of a wider range of environments available between water and DMSO phases within this regime.[6,50] In particular, FA has shown increased inhomogeneity as a result of stronger interactions with water.[51] Finally, above 40 mol %, the solution again becomes more homogeneous in the DMSO-rich regime, which is consistent with previous measurements.[7,29,44]

The decrease in heterogeneity also correlates with our previous study showing that above 35 mol %, DMSO phase-separates into an "aggregate", which removes DMSO molecules from the water phase, and this produces a more homogeneous environment.[41]

Time constants (τ, Figure 4A) represent the frequency fluctuation rates from H-bond dynamics and can be considered a probe of H-bond lifetimes.[42] In pure water, the relaxation of both probes is rapid: FA shows a decay of 0.71 ps, and DMF of 0.74 ps. These relaxation time constants fall within the range of literature values of 400 fs and 1 ps for *N*-methylacetamide (NMA).[5,46−48] These two time scales are commonly interpreted as local fluctuations of H-bond configurations followed by local reorganization of waters around the carbonyl group, respectively. Here, spectral diffusion rates are, however, monoexponential (Figure S5). To explore the effect of spectral diffusion due to reorientation of the probes, we have performed NLS analysis of spectra collected in the parallel and perpendicular polarization configurations. The nearly identical decays suggest that the dynamics arise from reorganization of the solvent, usually described as structural spectral diffusion (SSD), and the

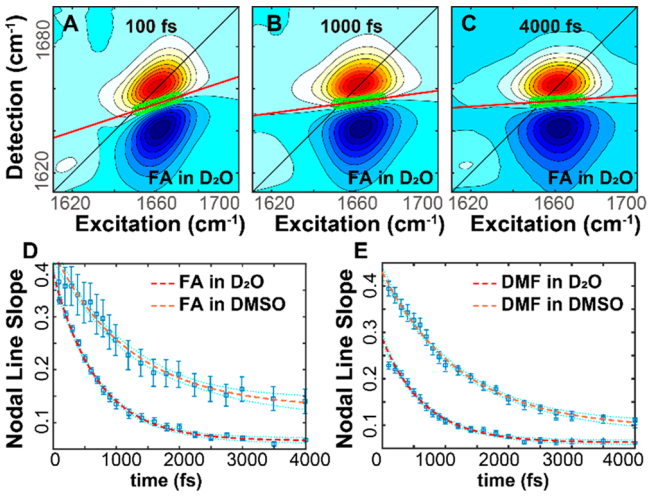

Figure 3. Representative 2D IR spectra of FA in D_2O at (A) 150 fs, (B) 1000 fs, and (C) 4000 fs. The center lines of the ground-state bleaches are highlighted in green. NLS decays of FA (D) and DMF (E) are shown along with the best-fit curves to the Bloch model (eq 1).

https://dx.doi.org/10.1021/acs.jpclett.0c00378
J. Phys. Chem. Lett. 2020, 11, 1903−1908

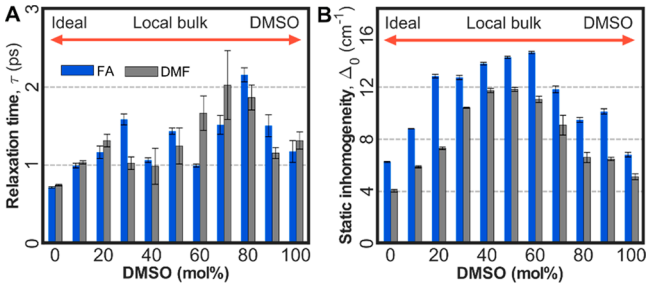

Figure 4. (A) Relaxation time constants, τ, and (B) static inhomogeneity, Δ_0, in FA (blue) and DMF (gray) as a function of DMSO concentration. The values are shown in Table S1.

decay contribution from the reorientation of the probe is small.[52]

Bimodal patterns across the concentration range can be observed for both FA and DMF. The dynamics slow down around 10−20 mol %, become faster around 30−50 mol %, and finally slow again above 50 mol %. These trends can be interpreted as follows: (1) Low DMSO concentrations (<20 mol %) produce homogeneous, ideal-solution-like environments where the local dynamics correlate with bulk viscosity. A critical point is reached around 20 mol % where the solution begins to deviate from ideal behavior. This is the concentration range in which DMSO−water interactions peak with the 1 HB population maximized.[41] Bulk properties, such as entropy of mixing, also begin to deviate from ideal behavior around 20 mol % (Figure S6). (2) Intermediate concentrations (20−50 mol %) produce faster dynamics, as DMSO forms clusters, resulting in a locally homogeneous environment for the DMSO-rich and water-rich domains. This phase segregation allows for faster H-bond dynamics provided that the probes are primarily localized to one of the domains. We have labeled this regime "local bulk", suggesting that water H-bond networks are bulk-like in the water-rich phase. (3) Above 40 mol % the dynamics slow down as the solution again becomes more homogeneous, but different from the low concentration regime, as the solution becomes more ideal in the DMSO-rich regime.

These results point toward overall more heterogeneous environments at intermediate concentrations, in line with previous studies,[7,44] but the local dynamics become faster as a result of phase separation. This indicates that the H-bonds between water molecules may be less perturbed within this concentration range because of clustering within both DMSO and water components. This "saddle-shaped" pattern (Figure 4A) is similar to what has been reported for the wobbling-in-a-cone motions of water,[7] which suggest that dynamics are faster around 50 mol % DMSO compared to other concentrations. 2D IR experiments have also observed accelerated spectral diffusion around 50 mol %, although the reported differences are less pronounced.[7] Our results are consistent with recent anisotropy studies by Bakker and co-workers, indicating DMSO−water H-bonds may become more labile at higher concentrations.[53]

Finally, we interpret the differences in relaxation rates between FA and DMF (Figure 4A). In water, both FA and DMF show similar dynamics. Above 20−30 mol %, both probes begin to exhibit faster dynamics, but DMF shows the fastest dynamics at 40 mol %, whereas FA shows minima at 40 and 60 mol %. This indicates that FA may be localized to a water-rich shell around 50 mol %, while DMF, because of its lower polarity, localizes either to the DMSO phase or the interface between components, thus exhibiting slower dynamics at 60 mol %. Static inhomogeneity indicates that FA exhibits a more heterogeneous environment, which could be the result of partially disrupted H-bond networks in the water phase, whereas DMF samples more homogeneous environments. FTIR line widths (Figure S2) are broader for FA across the concentration range with maxima around 30 and 80 mol %, whereas DMF shows a smoother trend reaching a maximum width around 40 mol % DMSO. We have recently shown that despite FA's ability to donate H-bonds through its $-NH_2$ group, H-bonds involving the amine do not perturb the carbonyl frequency,[51] ruling out the additional H-bonds as a source of spectral inhomogeneity. Together, the FTIR and 2D IR spectra indicate that FA samples more heterogeneous polar environments.

In summary, experiments indicate the following: (1) Fast dynamics are not correlated with "static" inhomogeneity; instead, faster dynamics appear within the "bulk like" regime where the inhomogeneous contribution to the line shape is largest. (2) FA and DMF experience different solvation environments as a result of their polarities, though qualitatively the trends are similar. We postulate that water H-bond networks can remain mostly intact at intermediate concentrations because of clustering due to preferential DMSO−DMSO interactions, which reduces the number of DMSO−water interactions, thus increasing the water−water interactions and producing a more bulk-like environment. This is in agreement with the previous description of DMSO H-bond populations in mixtures.[41] Next, we provide a molecular interpretation of these experimental observations through MD simulations.

Clustering in DMSO−Water Mixtures. MD simulations enable us to examine the degree of molecular segregation through the H-bond networks of water (section S5 and Figure S7). These MD simulations have been benchmarked across the 0−100 mol % DMSO concentration range in a recent publication.[49] Here we focus on the 0−70 mol % range as beyond this concentration the cluster size remains constant (see Figure S7C). In brief, MD coordinates are used to compute an H-bond network for each snapshot. Figure 5A shows a representation of a network constructed from a snapshot of 30 mol % DMSO. In the network, individual waters are represented as nodes, and each pair sharing an H-bond is connected by an edge. Visually inspecting the network layout shows the appearance of a hub-and-spoke-like topology with a central group of water molecules surrounded by smaller clusters which contain between 2 and ∼50 molecules. These peripheral clusters are connected to the rest of the network by only a few edges. To quantify the degree of clustering, we compute the network entropy using standard graph theory methods (section S5). Uniform networks, where the average number of edges is similar for each node, exhibit lower entropy.[16] Below 30 mol %, the H-bond entropy is lower compared to ideal solutions, indicating that water retains its characteristic networks throughout the 0−30 mol % concentration range and supporting the interpretation of the local bulk regime observed in the experiment. The results show that water H-bond networks are less disrupted compared to an ideal solution as a result of clustering, which explains the faster NLS decays observed in the intermediate concentration range. Participation ratios measure of the size of the water H-bond network. In bulk water, each cluster contains ∼120 molecules. The value is reduced to ∼25 molecules and remains relatively constant above 30 mol % DMSO.

Multiscale Relaxation of Water Networks. We compute the H-bond network identity (HNI) using eq S8. In brief, at each time step the network is projected onto the initial network, analogous

https://dx.doi.org/10.1021/acs.jpclett.0c00378
J. Phys. Chem. Lett. 2020, 11, 1903−1908

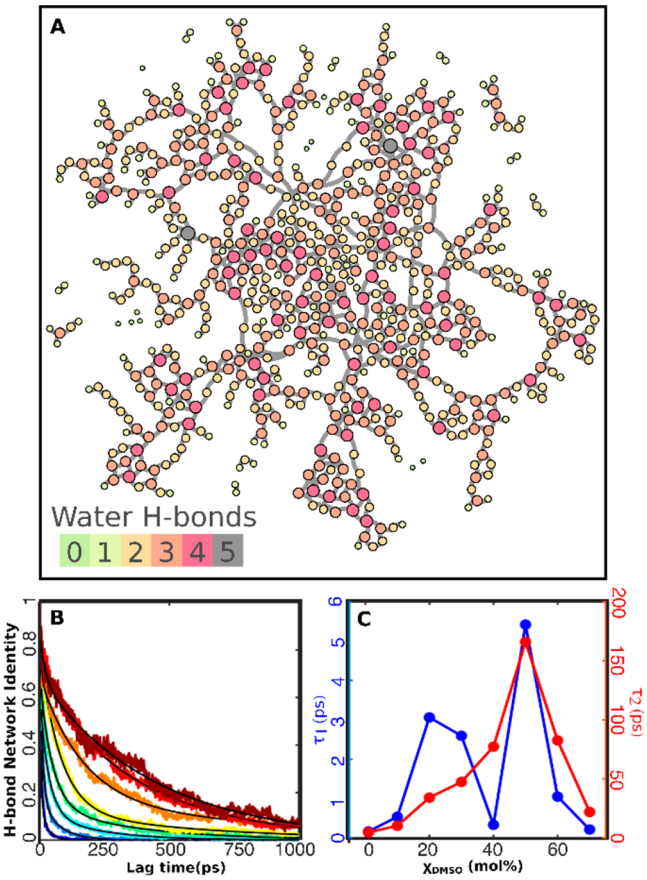

Figure 5. (A) Water−water H-bond network constructed from an MD snapshot at 30 mol % DMSO, shown for illustration. Each water molecule is represented by a node (circles). H-bonded molecules are connected by edges (curved lines) and placed in closer proximity in the two-dimensional layout. Each node is color-coded by the number of connections to other nodes (i.e., H-bonds). The layout is generated using the ForceAtlas2 algorithm.[54] (B) Water H-bond network relaxation as a function of DMSO concentration from 0 to 70% in 10% intervals as indicated by the blue to red curves. The black solid lines represent triexponential fits to the data (see section S5.5). (C) Decay constants for the fast (τ_1) and intermediate (τ_2) time constants from the exponential fits, as a function of DMSO concentrations. The slowest component is shown in Figure S9.

to an autocorrelation (Figure 5B,C and section S5). Given the high dimensionality of the space, the network identity value decreases as the original H-bonds are broken and new ones are formed. We observe that the relaxation is multiexponential, with dynamics observed on three separate time scales: (1) Picosecond initial breaking and reforming of H-bonds without substantial rearrangement of water molecules account for 10−20% of the overall relaxation. In particular, bulk-water-like time scales of 150−500 fs are observed at low and medium DMSO concentrations. Interestingly, fast network dynamics (Figure 5C) show the same fast−slow−fast−slow behavior as observed in the 2D IR dynamics (Figure 4B) with the fastest dynamics in the intermediate regime occurring around 40 mol %, in agreement with experiment. These observations are consistent with the concentration-dependent 2D IR spectral diffusion rates of FA and DMF described above and are also in agreement with the time scale of previous ultrafast studies of water and NMA dynamics.[48,55,56] (2) Intermediate (<200 ps) dynamics can be attributed to redistribution of water molecules within each cluster. These relaxation processes follow a similar trend to the OHD-OKE measurement of the reorientational dynamics and 2D IR spectral diffusion of water,[7] which are also consistent with previous studies.[27,29,44] Naturally, these intermediate time scales cannot be reached with 2D IR experiments because of the picosecond vibrational lifetime of the carbonyl probes. (3) Finally, the long time scale component (∼100−1000 ps) follows trends similar to the <200 ps component, showing the slowest relaxation within intermediate concentration regimes. Together, these results are consistent with the extensive literature on DMSO−water dynamics, such as 2D IR,[7,44] MD simulations,[39] fluorescence spectroscopy,[43] and NMR spin relaxation.[29] Subpicosecond and picosecond relaxation rates appear to occur on similar time scales as reported for an ester carbonyl probe in the same mixtures, although the patterns are qualitatively different because those studies did not find changes in the C=O−HOH hydrogen-bond switching rates above 15 mol % DMSO.[42] Together, the experiments and simulations paint a more complete picture of H-bond network relaxation in clustered environments, suggesting that H-bond rearrangement and diffusion of water molecules within each cluster are responsible for the dynamics observed by various measurements.

Studies presented here provide the first probe-dependent measurement of solvation dynamics and allow us to specifically quantify differences between environments. Simulations begin to produce a unified view of dynamics in DMSO−water mixtures over a range of time scales. Together with the network analysis, we show that clustering and heterogeneity produce dynamics on multiple time scales. In brief, the findings are as follows: (1) Subpicosecond dynamics become faster in the intermediate DMSO concentration regime, while static heterogeneity increases. We have termed this regime the local bulk to explain the bulk-like behavior of water within the clusters while retaining the overall heterogeneity of the mixture. (2) The size of the water clusters at 30 mol % is approximately 25 molecules on average and is independent of DMSO concentration above this range. (3) Different probes (FA and DMF) sample different environments. These observations resolve the differences between previous experiments and imply that spectroscopic measurements involving extrinsic probes must be interpreted in this light. (4) Dynamical information is consistent with ensemble H-bond populations described previously.[41] (5) H-bond networks relax on at least three distinct time scales. Finally, the methods presented here will be useful for further developing an intuitive picture of mixtures of amphiphilic molecules, which is crucial to understanding a wide range of complex phenomena, such as biological compartmentalization, as well as the unique physical properties of amphiphilic mixtures.[11] For example, recent simulations suggest increased proton transport rates in aqueous−organic mixtures as a result of wire-like connections between waters, despite the slow reorientation of water in the mixtures, which decreases proton mobility.[57] Our results begin to explain the interactions that produce such unique properties.

EXPERIMENTAL METHODS

Detailed descriptions are provided in the Supporting Information.

FTIR and 2D IR Spectroscopy. Concentration-dependent FTIR spectra were measured at room temperature with 1 cm^{-1} resolution. All solvents were used as received. Two-

https://dx.doi.org/10.1021/acs.jpclett.0c00378
J. Phys. Chem. Lett. 2020, 11, 1903−1908

dimensional infrared (2D IR) spectra were acquired using a pulse-shaper-based spectrometer.[58]

Molecular Dynamics Simulations. MD simulations were carried out using a modified CHARMM General force-field for DMSO, formamide, and DMF, along with the tip4p/ew model for water benchmarked in a recent paper.[49] In brief, the MD box was packed using random initial positions and equilibrated for 15 ns in an *NPT* ensemble followed by a 5 ns production run.

Hydrogen Bond Network Analysis. Water−water H-bonds were determined by two adjacent water molecules with an O−O distance of <3.4 Å and an H−O−O angle of <30°. The percentage of bulk water, average participation ratio, network entropy, and tetrahedral order parameters were defined by network analysis using an adjacency matrix and relative geometries as described in section S5.

■ ASSOCIATED CONTENT

Supporting Information

The Supporting Information is available free of charge at https://pubs.acs.org/doi/10.1021/acs.jpclett.0c00378.

Experimental procedures, including sample preparation and IR measurements, 2D IR measurements, entropy of mixing, MD simulation protocols, and analysis of results; additional figures referenced in the text (PDF)

■ AUTHOR INFORMATION

Corresponding Author

Carlos R. Baiz − *Department of Chemistry, University of Texas at Austin, Austin, Texas 78712-1224, United States;* orcid.org/0000-0003-0699-8468; Email: cbaiz@cm.utexas.edu

Authors

Kwang-Im Oh − *Department of Chemistry, University of Texas at Austin, Austin, Texas 78712-1224, United States*

Xiao You − *Department of Chemistry, University of Texas at Austin, Austin, Texas 78712-1224, United States*

Jennifer C. Flanagan − *Department of Chemistry, University of Texas at Austin, Austin, Texas 78712-1224, United States*

Complete contact information is available at: https://pubs.acs.org/10.1021/acs.jpclett.0c00378

Author Contributions

†K.-I.O. and X.Y. contributed equally to this work.

Notes

The authors declare no competing financial interest.

■ ACKNOWLEDGMENTS

We acknowledge research grants from the Welch Foundation (F-1891) and the National Science Foundation (CHE-1847199). Simulations were carried out at the Texas Advanced Computing Center (TACC). This is a Plan II SAWIAGOS Project. We thank Prof. Michael Fayer for useful advice on measuring polarization-dependent 2D IR spectra.

■ REFERENCES

(1) Dixit, S.; Crain, J.; Poon, W. C. K.; Finney, J. L.; Soper, A. K. Molecular segregation observed in a concentrated alcohol-water solution. *Nature* **2002**, *416* (6883), 829−832.

(2) Ghoraishi, M. S.; Hawk, J. E.; Phani, A.; Khan, M. F.; Thundat, T. Clustering mechanism of ethanol-water mixtures investigated with photothermal microfluidic cantilever deflection spectroscopy. *Sci. Rep.* **2016**, *6* (1), 23966.

(3) Mochizuki, K.; Pattenaude, S. R.; Ben-Amotz, D. Influence of Cononsolvency on the Aggregation of Tertiary Butyl Alcohol in Methanol-Water Mixtures. *J. Am. Chem. Soc.* **2016**, *138* (29), 9045−9048.

(4) Lenton, S.; Rhys, N. H.; Towey, J. J.; Soper, A. K.; Dougan, L. Temperature-Dependent Segregation in Alcohol-Water Binary Mixtures Is Driven by Water Clustering. *J. Phys. Chem. B* **2018**, *122* (32), 7884−7894.

(5) Salamatova, E.; Cunha, A. V.; Bloem, R.; Roeters, S. J.; Woutersen, S.; Jansen, T. L. C.; Pshenichnikov, M. S. Hydrophobic Collapse in N-Methylacetamide−Water Mixtures. *J. Phys. Chem. A* **2018**, *122* (9), 2468−2478.

(6) Daschakraborty, S. How do glycerol and dimethyl sulfoxide affect local tetrahedral structure of water around a nonpolar solute at low temperature? Importance of preferential interaction. *J. Chem. Phys.* **2018**, *148* (13), 134501.

(7) Wong, D. B.; Sokolowsky, K. P.; El-Barghouthi, M. I.; Fenn, E. E.; Giammanco, C. H.; Sturlaugson, A. L.; Fayer, M. D. Water dynamics in water/DMSO binary mixtures. *J. Phys. Chem. B* **2012**, *116* (18), 5479−5490.

(8) Hansen, J. S.; Thompson, J. R.; Hélix-Nielsen, C.; Malmstadt, N. Lipid directed intrinsic membrane protein segregation. *J. Am. Chem. Soc.* **2013**, *135* (46), 17294−17297.

(9) Horta, B. A. C.; Hünenberger, P. H. Enantiomeric Segregation in the Gel Phase of Lipid Bilayers. *J. Am. Chem. Soc.* **2011**, *133* (22), 8464−8466.

(10) Kraft, M. L.; Weber, P. K.; Longo, M. L.; Hutcheon, I. D.; Boxer, S. G. Phase separation of lipid membranes analyzed with high-resolution secondary ion mass spectrometry. *Science* **2006**, *313* (5795), 1948−1951.

(11) Boeynaems, S.; Alberti, S.; Fawzi, N. L.; Mittag, T.; Polymenidou, M.; Rousseau, F.; Schymkowitz, J.; Shorter, J.; Wolozin, B.; Van Den Bosch, L.; Tompa, P.; Fuxreiter, M. Protein Phase Separation: A New Phase in Cell Biology. *Trends Cell Biol.* **2018**, *28* (6), 420−435.

(12) Towey, J. J.; Soper, A. K.; Dougan, L. Molecular insight into the hydrogen bonding and micro-segregation of a cryoprotectant molecule. *J. Phys. Chem. B* **2012**, *116* (47), 13898−13904.

(13) Vieregg, J. R.; Lueckheide, M.; Marciel, A. B.; Leon, L.; Bologna, A. J.; Rivera, J. R.; Tirrell, M. V. Oligonucleotide-Peptide Complexes: Phase Control by Hybridization. *J. Am. Chem. Soc.* **2018**, *140* (5), 1632−1638.

(14) Nandi, S.; Parui, S.; Halder, R.; Jana, B.; Bhattacharyya, K. Interaction of proteins with ionic liquid, alcohol and DMSO and in situ generation of gold nano-clusters in a cell. *Biophys. Rev.* **2018**, *10* (3), 757−768.

(15) Chen, S.; Yan, T.; Fischer, M.; Mordvinkin, A.; Saalwächter, K.; Thurn-Albrecht, T.; Binder, W. H. Opposing Phase-Segregation and Hydrogen-Bonding Forces in Supramolecular Polymers. *Angew. Chem., Int. Ed.* **2017**, *56* (42), 13016−13020.

(16) Choi, J.-H.; Lee, H.; Choi, H. R.; Cho, M. Graph Theory and Ion and Molecular Aggregation in Aqueous Solutions. *Annu. Rev. Phys. Chem.* **2018**, *69*, 125−149.

(17) Lim, J.; Park, K.; Lee, H.; Kim, J.; Kwak, K.; Cho, M. Nanometric Water Channels in Water-in-Salt Lithium Ion Battery Electrolyte. *J. Am. Chem. Soc.* **2018**, *140* (46), 15661−15667.

(18) Rao, F.; Garrett-Roe, S.; Hamm, P. Structural inhomogeneity of water by complex network analysis. *J. Phys. Chem. B* **2010**, *114* (47), 15598−15604.

(19) Roos, M.; Ott, M.; Hofmann, M.; Link, S.; Rössler, E.; Balbach, J.; Krushelnitsky, A.; Saalwächter, K. Coupling and Decoupling of Rotational and Translational Diffusion of Proteins under Crowding Conditions. *J. Am. Chem. Soc.* **2016**, *138* (32), 10365−10372.

(20) Senske, M.; Törk, L.; Born, B.; Havenith, M.; Herrmann, C.; Ebbinghaus, S. Protein stabilization by macromolecular crowding through enthalpy rather than entropy. *J. Am. Chem. Soc.* **2014**, *136* (25), 9036−9041.

(21) Mountain, R. D.; Thirumalai, D. Molecular Dynamics Simulations of End-to-End Contact Formation in Hydrocarbon Chains

in Water and Aqueous Urea Solution. *J. Am. Chem. Soc.* **2003**, *125* (7), 1950−1957.
(22) Lewis, J. K.; Bischof, J. C.; Braslavsky, I.; Brockbank, K. G. M.; Fahy, G. M.; Fuller, B. J.; Rabin, Y.; Tocchio, A.; Woods, E. J.; Wowk, B. G.; Acker, J. P.; Giwa, S. The Grand Challenges of Organ Banking: Proceedings from the first global summit on complex tissue cryopreservation. *Cryobiology* **2016**, *72* (2), 169−182.
(23) Notman, R.; Noro, M.; O'Malley, B.; Anwar, J. Molecular basis for dimethylsulfoxide (DMSO) action on lipid membranes. *J. Am. Chem. Soc.* **2006**, *128* (43), 13982−13983.
(24) Zhang, X.; Zhu, Y.; Granick, S. Hydrophobicity at a Janus interface. *Science* **2002**, *295* (5555), 663−666.
(25) Cowie, J. M. G.; Toporowski, P. M. Association in the binary liquid system dimethyl sulfoxide−water. *Can. J. Chem.* **1961**, *39* (11), 2240−2243.
(26) LeBel, R. G.; Goring, D. A. I. Density, Viscosity, Refractive Index, and Hygroscopicity of Mixtures of Water and Dimethyl Sulfoxide. *J. Chem. Eng. Data* **1962**, *7* (1), 100−101.
(27) Catalán, J.; Díaz, C.; García-Blanco, F. Characterization of Binary Solvent Mixtures of DMSO with Water and Other Cosolvents. *J. Org. Chem.* **2001**, *66* (17), 5846−5852.
(28) Clever, H. L.; Pigott, S. P. Enthalpies of mixing of dimethylsulfoxide with water and with several ketones at 298.15 K. *J. Chem. Thermodyn.* **1971**, *3* (2), 221−225.
(29) Packer, K. J.; Tomlinson, D. J. Nuclear spin relaxation and self-diffusion in the binary system, dimethylsulfoxide (DMSO)+ water. *Trans. Faraday Soc.* **1971**, *67* (0), 1302−13.
(30) Rasmussen, D. H.; MacKenzie, A. P. Phase Diagram for the System Water−Dimethylsulfoxide. *Nature* **1968**, *220* (5174), 1315−1317.
(31) Soper, A. K.; Luzar, A. A neutron diffraction study of dimethyl sulfoxide−water mixtures. *J. Chem. Phys.* **1992**, *97* (2), 1320−1331.
(32) Soper, A. K.; Luzar, A. Orientation of Water Molecules around Small Polar and Nonpolar Groups in Solution: A Neutron Diffraction and Computer Simulation Study. *J. Phys. Chem.* **1996**, *100* (4), 1357−1367.
(33) Lu, Z.; Manias, E.; Macdonald, D. D.; Lanagan, M. Dielectric Relaxation in Dimethyl Sulfoxide/Water Mixtures Studied by Microwave Dielectric Relaxation Spectroscopy. *J. Phys. Chem. A* **2009**, *113* (44), 12207−12214.
(34) Luzar, A.; Stefan, J. Dielectric behaviour of DMSO-water mixtures. A hydrogen-bonding model. *J. Mol. Liq.* **1990**, *46*, 221−238.
(35) Kashid, S. M.; Jin, G. Y.; Bagchi, S.; Kim, Y. S. Cosolvent Effects on Solute-Solvent Hydrogen-Bond Dynamics: Ultrafast 2D IR Investigations. *J. Phys. Chem. B* **2015**, *119* (49), 15334−15343.
(36) Wallace, V. M.; Dhumal, N. R.; Zehentbauer, F. M.; Kim, H. J.; Kiefer, J. Revisiting the Aqueous Solutions of Dimethyl Sulfoxide by Spectroscopy in the Mid- and Near-Infrared: Experiments and Car-Parrinello Simulations. *J. Phys. Chem. B* **2015**, *119* (46), 14780−14789.
(37) Wulf, A.; Ludwig, R. Structure and dynamics of water confined in dimethyl sulfoxide. *ChemPhysChem* **2006**, *7* (1), 266−272.
(38) Banik, D.; Kundu, N.; Kuchlyan, J.; Roy, A.; Banerjee, C.; Ghosh, S.; Sarkar, N. Picosecond solvation dynamics—A potential viewer of DMSO—Water binary mixtures. *J. Chem. Phys.* **2015**, *142* (5), 054505−11.
(39) Roy, S.; Bagchi, B. Solvation dynamics of tryptophan in water-dimethyl sulfoxide binary mixture: in search of molecular origin of composition dependent multiple anomalies. *J. Chem. Phys.* **2013**, *139* (3), 034308.
(40) Vishnyakov, A.; Lyubartsev, A. P.; Laaksonen, A. Molecular Dynamics Simulations of Dimethyl Sulfoxide and Dimethyl Sulfoxide−Water Mixture. *J. Phys. Chem. A* **2001**, *105* (10), 1702−1710.
(41) Oh, K.-I.; Rajesh, K.; Stanton, J. F.; Baiz, C. R. Quantifying Hydrogen-Bond Populations in Dimethyl Sulfoxide/Water Mixtures. *Angew. Chem., Int. Ed.* **2017**, *56* (38), 11375−11379.
(42) Kashid, S. M.; Jin, G. Y.; Chakrabarty, S.; Kim, Y. S.; Bagchi, S. Two-Dimensional Infrared Spectroscopy Reveals Cosolvent-Composition-Dependent Crossover in Intermolecular Hydrogen-Bond Dynamics. *J. Phys. Chem. Lett.* **2017**, *8*, 1604−1609.
(43) Ghosh, S.; Chattoraj, S.; Chowdhury, R.; Bhattacharyya, K. Structure and dynamics of lysozyme in DMSO−water binary mixture: fluorescence correlation spectroscopy. *RSC Adv.* **2014**, *4*, 14378−14384.
(44) Wei, Q.; Zhou, D.; Li, X.; Chen, Y.; Bian, H. Structural Dynamics of Dimethyl Sulfoxide Aqueous Solutions Investigated by Ultrafast Infrared Spectroscopy: Using Thiocyanate Anion as a Local Vibrational Probe. *J. Phys. Chem. B* **2018**, *122*, 12131.
(45) Bakulin, A. A.; Liang, C.; la Cour Jansen, T.; Wiersma, D. A.; Bakker, H. J.; Pshenichnikov, M. S. Hydrophobic Solvation: A 2D IR Spectroscopic Inquest. *Acc. Chem. Res.* **2009**, *42* (9), 1229−1238.
(46) Cunha, A. V.; Salamatova, E.; Bloem, R.; Roeters, S. J.; Woutersen, S.; Pshenichnikov, M. S.; Jansen, T. L. C. Interplay between Hydrogen Bonding and Vibrational Coupling in Liquid N-Methylacetamide. *J. Phys. Chem. Lett.* **2017**, *8* (11), 2438−2444.
(47) DeCamp, M. F.; DeFlores, L.; McCracken, J. M.; Tokmakoff, A.; Kwac, K.; Cho, M. Amide I Vibrational Dynamics of N-Methylacetamide in Polar Solvents: The Role of Electrostatic Interactions. *J. Phys. Chem. B* **2005**, *109* (21), 11016−11026.
(48) Hamm, P.; Lim, M.; Hochstrasser, R. M. Structure of the Amide I Band of Peptides Measured by Femtosecond Nonlinear-Infrared Spectroscopy. *J. Phys. Chem. B* **1998**, *102* (31), 6123−6138.
(49) Oh, K.-I.; Baiz, C. R. Empirical S= O stretch vibrational frequency map. *J. Chem. Phys.* **2019**, *151* (23), 234107.
(50) Perera, A.; Mazighi, R. On the nature of the molecular ordering of water in aqueous DMSO mixtures. *J. Chem. Phys.* **2015**, *143* (15), 154502.
(51) Oh, K.-I.; Baiz, C. R. Crowding stabilizes DMSO−water hydrogen-bonding interactions. *J. Phys. Chem. B* **2018**, *122* (22), 5984−5990.
(52) Kramer, P. L.; Nishida, J.; Giammanco, C. H.; Tamimi, A.; Fayer, M. D. Observation and theory of reorientation-induced spectral diffusion in polarization-selective 2D IR spectroscopy. *J. Chem. Phys.* **2015**, *142* (18), 184505.
(53) Lotze, S.; Groot, C. C. M.; Vennehaug, C.; Bakker, H. J. Femtosecond Mid-Infrared Study of the Dynamics of Water Molecules in Water−Acetone and Water−Dimethyl Sulfoxide Mixtures. *J. Phys. Chem. B* **2015**, *119* (16), 5228−5239.
(54) Jacomy, M.; Venturini, T.; Heymann, S.; Bastian, M. ForceAtlas2, a Continuous Graph Layout Algorithm for Handy Network Visualization Designed for the Gephi Software. *PLoS One* **2014**, *9* (6), e98679−12.
(55) Perakis, F.; De Marco, L.; Shalit, A.; Tang, F.; Kann, Z. R.; Kühne, T. D.; Torre, R.; Bonn, M.; Nagata, Y. Vibrational Spectroscopy and Dynamics of Water. *Chem. Rev.* **2016**, *116* (13), 7590−7607.
(56) Ramasesha, K.; De Marco, L.; Mandal, A.; Tokmakoff, A. Water vibrations have strongly mixed intra- and intermolecular character. *Nat. Chem.* **2013**, *5* (11), 935−940.
(57) Liang, C.; Jansen, T. L. C. Proton transport in a binary biomimetic solution revealed by molecular dynamics simulation. *J. Chem. Phys.* **2011**, *135* (11), 114502−9.
(58) Edington, S. C.; Gonzalez, A.; Middendorf, T. R.; Halling, D. B.; Aldrich, R. W.; Baiz, C. R. Coordination to lanthanide ions distorts binding site conformation in calmodulin. *Proc. Natl. Acad. Sci. U. S. A.* **2018**, *115* (14), E3126−E3134.

https://dx.doi.org/10.1021/acs.jpclett.0c00378
J. Phys. Chem. Lett. 2020, 11, 1903−1908